CHEMISTRY OF MATERIALS

Article

pubs.acs.org/cm

Structural Evolution of Electrochemically Lithiated MoS_2 Nanosheets and the Role of Carbon Additive in Li-Ion Batteries

Chandramohan George,*[,†,§] Andrew J. Morris,*[,∥,§] Mohammad H. Modarres,[†] and Michael De Volder*[,†]

[†]Institute for Manufacturing, Department of Engineering, University of Cambridge, 17 Charles Babbage Road, Cambridge CB3 0FS, United Kingdom

[∥]Theory of Condensed Matter Group, Cavendish Laboratory, University of Cambridge, J. J. Thomson Avenue, Cambridge CB3 0HE, United Kingdom

Supporting Information

ABSTRACT: Understanding the structure and phase changes associated with conversion-type materials is key to optimizing their electrochemical performance in Li-ion batteries. For example, molybdenum disulfide (MoS_2) offers a capacity up to 3-fold higher (~1 Ah/g) than the currently used graphite anodes, but they suffer from limited Coulombic efficiency and capacity fading. The lack of insights into the structural dynamics induced by electrochemical conversion of MoS_2 still hampers its implementation in high energy-density batteries. Here, by combining *ab initio* density-functional theory (DFT) simulation with electrochemical analysis, we found new sulfur-enriched intermediates that progressively insulate MoS_2 electrodes and cause instability from the first discharge cycle. Because of this, the choice of conductive additives is critical for the battery performance. We investigate the mechanistic role of carbon additive by comparing equal loading of standard Super P carbon powder and carbon nanotubes (CNTs). The latter offer a nearly 2-fold increase in capacity and a 45% reduction in resistance along with Coulombic efficiency of over 90%. These insights into the phase changes during MoS_2 conversion reactions and stabilization methods provide new solutions for implementing cost-effective metal sulfide electrodes, including Li−S systems in high energy-density batteries.

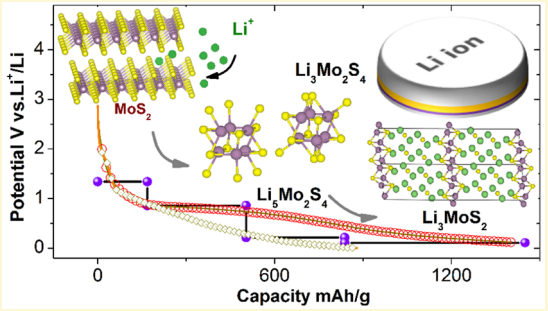

Layered transition metal dichacogenides[1] (MX_2 where M = Mo, W, Ti; X = S, Se, Te) have recently been applied in solar cells,[2] photodetectors,[3] hydrogen storage,[4] catalysis,[5] Li-ion battery,[6] supercapacitors,[7] transistors,[8] and lubricants.[9] For Li-ion batteries, MoS_2 offers almost 3-fold improvement in capacity[10,11] (>800−1000 mAh/g) compared to currently used graphite anodes[12] (theoretical capacity ~370 mAh/g). MoS_2 comprises sandwiched S−Mo−S layers with an interlayer spacing[13] of ~6.7 Å, which allows Li-ion insertion[14] between layers, similar to graphite. However, in MoS_2 electrodes, from ~1.1 V versus Li^+/Li onward, Li^+-ions begin to react with sulfur atoms, and MoS_2 gradually changes from a trigonal prismatic (2H-MoS_2) to an octahedral (1T-Li_xMoS_2) phase.[15] After this phase transition, conversion reactions are intensified at ~0.5 V versus Li^+/Li, causing MoS_2 to fragment and disintegrate into LiS_2 and Mo nanoparticles. When these reactions coincide with electrolyte decomposition (~0.5−0.1 V), most of the electrode turns into a gel-like matrix containing Mo nanoparticles. The overall reaction typically leads to low capacity and poor columbic efficiency because, after reactions with Li^+-ions, MoS_2 electrodes are enriched with polysulfide species (as reaction products), and partially dissolve in the battery electrolyte.[16,17] Low electron conductivity is particularly problematic with the use of standard conductive additives (e.g., carbon particles ~50−200 nm in diameter), which tend to lose electrical contact with the active particles during the conversion reactions. In order to mitigate these shortcomings, carbon nanotubes (CNTs) have been investigated as a conductive additive resulting in composites with improved electronic conductivity.[18,19] Despite suggested drawbacks related to multiwalled carbon nanotubes (MWCNTs) shedding carbon layers[20] and leading to an increase in solid−electrolyte interface (SEI), CNTs offer superior electrochemical performance as conductive additives. For example, CNT-MoS_2 sheets[21] were shown to offer a capacity of ~512 mAh/g at 100A/g, and the highest first cycle capacity was reported for MoS_2-MWCNTs[20] composites reaching up to ~2774 mAh/g at 100 mA/g, and more recently, hierarchical MoS_2 tubular-CNT structures were shown to deliver 800 mAh/g at 5A/g (1000 cycles).[22] These values are larger than those reported for MoS_2/carbon nanoboxes,[23] MoS_2/polyaniline nanowires,[24] MoS_2 nanowall/cellulose,[25] MoS_2-graphene,[26] MoS_2-polyaniline,[24] MoS_2-carbon coatings,[27] MoS_2-highly ordered mesoporous carbon,[28] MoS_2-disordered graphene-like carbon,[29] and MoS_2 hierarchical structures.[14] Although this fact highlights CNT's commercial potential, it is still unclear how CNT additives cope with metal

Received: June 28, 2016
Revised: September 18, 2016
Published: September 19, 2016

DOI: 10.1021/acs.chemmater.6b02607
Chem. Mater. 2016, 28, 7304−7310

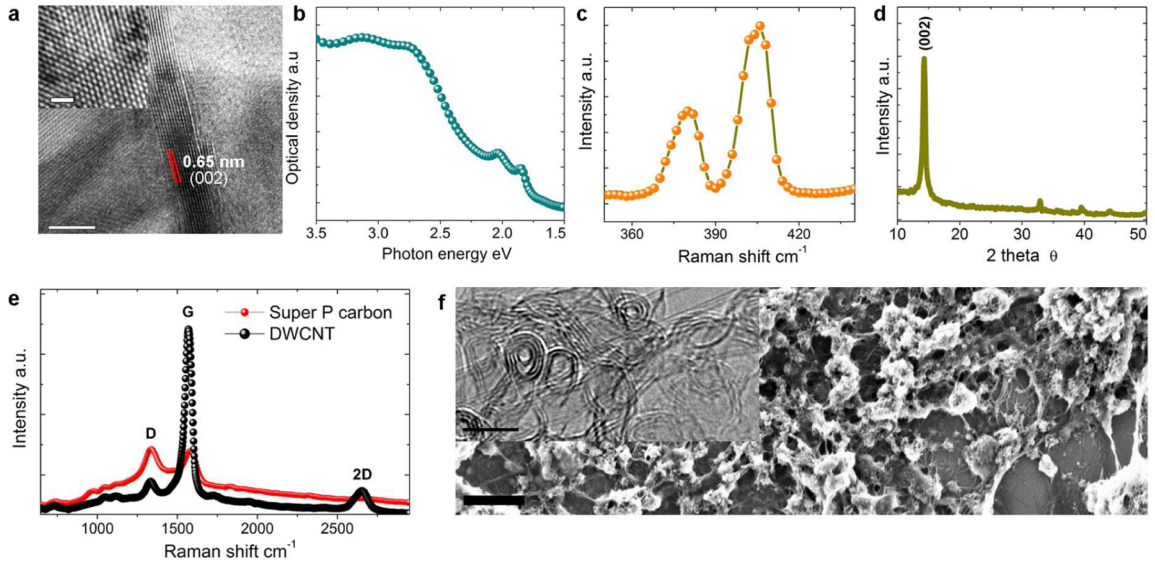

Figure 1. (a) High resolution transmission electron microscopic (HRTEM) image of an individual MoS_2 flake (scale bar 10 nm); inset showing MoS_2 atomic lattice (scale bar 1 nm). (b) UV−vis static absorption spectra of MoS_2 nanosheets. (c) Raman spectroscopic data show two characteristic peaks at 383 (E_{2g}^1) and 408 (A_{1g}) of MoS_2 sheets. (d) X-ray diffraction patterns obtained on MoS_2 samples indexed to molybdenite. (e) Raman spectra of Super P carbon and DWCNTs. (f) Scanning electron microscopic image of MoS_2-DWCNTs-PVDF composite diluted for imaging (scale bar 500 nm) with an inset showing HRTEM image of the commercial CNTs used in this work (inset scale bar 5 nm).

sulfide conversion reactions that cause large structural degradation and strain in electrodes during battery charge−discharge cycles. In order to understand this, we performed a detailed DFT analysis of likely intermediates that determine reversible and nonreversible reaction pathways during charge−discharge cycles. This is particularly challenging since the Li-MoS_2 reaction entails a wide range of off-stoichiometric/intermediate compounds that are short-lived and not often identified but yet significantly influence the battery capacity and rate performance.[30] For example, detection of Mo and Mo_xLi_y metallic nanoparticles in lithiated MoS_2 electrodes poses considerable difficulties because they tend to be considerably amorphous[31] and therefore go unnoticed even in *in situ* XRD measurements, whereas an *ab initio* density-functional theory (DFT) analysis[32] reported that, after lithiation of MoS_2, the reformation of MoS_2 from the converted mixture of Mo and LiS_2 is less energetically favorable, indicating that Li-MoS_2 is an irreversible reaction. It was also suggested using both DFT and electrochemical analysis that MoS_2-Li batteries behave similarly to lithium−sulfur (Li−S) batteries after the first discharge cycle. The exact reaction that metallic Mo nanoparticles undergo during successive cycles is however still not clear.

Our DFT based investigation performs structure searches from random starting atomic locations over a range of stoichiometries, complementing a previous study[28] which biased their predicted structures toward lithiated layered MoS_2 phases. Our approach ensures that the structures found are low in energy for a given stoichiometry, allowing the prediction of average voltages. They are highly likely to be thermally accessible at finite temperature and in a disordered system are likely to provide ground-state structural motifs.

By combing DFT simulation and electrochemical analysis we demonstrate that MoS_2-Li-ion battery electrodes inherently suffer from a progressive insulating behavior and structural instability from the first charge/discharge. Therefore, the choice of carbon additive which better mitigates the above issues is critical to the performance of these batteries. We carefully compared equal loading of Super P Carbon and commercial double wall carbon nanotubes (DWCNTs) as a conductive additive (≤10 wt %), see Experimental Section. We deduced that these 1D materials form an entangled network that confines the converted products in electrochemically active regions, which otherwise are degraded via reactions with the battery electrolyte as discussed earlier. This is evidenced by a 2-fold capacity enhancement and improved Coulombic efficiency compared to Super P carbon.

RESULTS AND DISCUSSION

As shown in Figure 1a, the MoS_2 sheets have an average thickness of ∼7 nm based on measuring tens of individual sheets in HRTEM while the lateral average dimensions are estimated to be around ∼100 nm. The UV−Vis static absorption data of MoS_2 dispersion is characteristic of excitons (A and B) originating in 2D MoS_2 nanosheets (Figure 1b) corresponding to photon energies (at ∼1.83−2.05 eV), while higher energies (at ∼2.5−2.9 eV) are associated with transitions taking place between the valence and conduction bands via deep states. Raman spectroscopic data show two characteristic peaks at ∼383 cm^{-1} (E_{2g}^1 in-plane mode) and ∼408 cm^{-1} (A_{1g} out-of-plane mode), consistent with the S−Mo−S vibration in MoS_2 (Figure 1c). The XRD patterns obtained from MoS_2 nanosheet films (on silicon substrates) can be indexed to pure phase MoS_2 as shown in Figure 1d. The samples were characterized to be fully crystalline, and neither side products nor different MoS_2 phases were detected. In Figure 1e the Raman spectra of DWCNTs and Super P carbon (∼50 nm nearly spherical particles) are compared, showing as expected a substantially higher G/D ratio for the DWCNTs. Finally, Figure 1f shows an SEM image of a DWCNT-MoS_2-PVDF slurry after dilution in hexane, casting and drying along with an inset TEM image of the pristine DWCNTs that are used as conductive additive.

Coin cell batteries (CR2032 type) were fabricated with MoS_2 nanosheet electrodes containing equal loading of either

DOI: 10.1021/acs.chemmater.6b02607
Chem. Mater. 2016, 28, 7304−7310

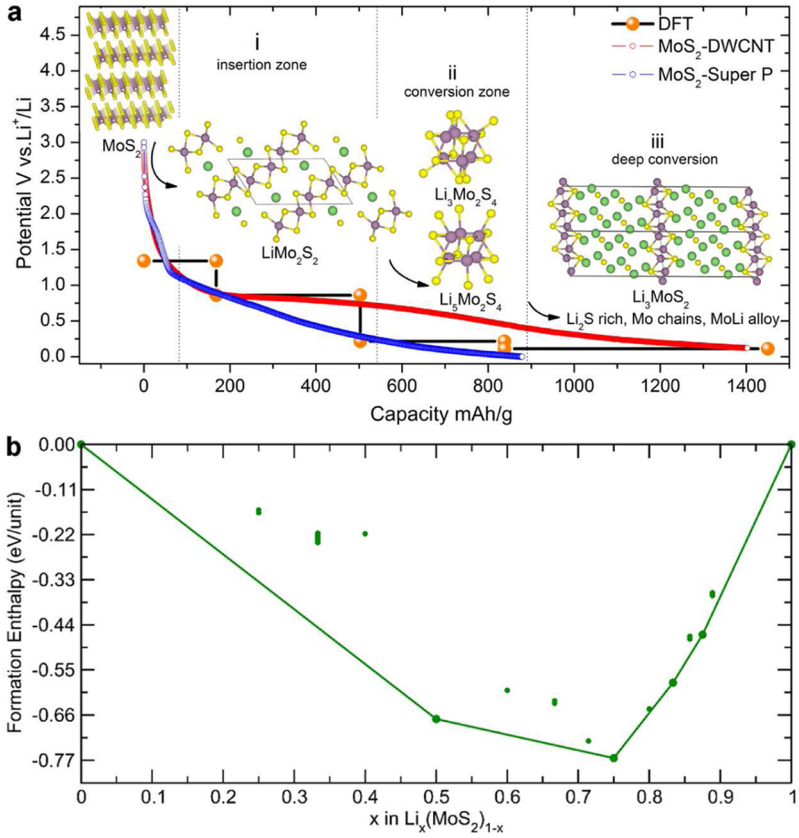

Figure 2. (a) Representative discharge profiles from the first cycle of MoS_2-DWCNT and MoS_2-Super P electrodes together with the average voltages calculated from DFT energies, relative to Li^+/Li and assuming each reaction is 2-phase: (i) For the metastable *Cmcm* symmetry $LiMo_2S_2$ phase, the sheets are buckled. (ii) For MoS_2, 2 clusters found in a sea of Li, the clusters $Li_3Mo_2S_4$ and $Li_5Mo_2S_4$ are found, with the sulfur being pulled away from Mo and toward the Li. (iii) The $P2_1/c$ symmetry Li_3MoS_2 leading to segregated Li_2S regions. (b) Density-functional theory (DFT) studies of MoS_2 electrodes, convex hull of the low energy $Li_x(MoS_2)_y$ structures found using AIRSS.

DWCNTs or conventional Super P carbon, and the electrode thickness was maintained at around ∼30 μm (see Supporting Information section S4). Figure 2a shows a typical discharge profile from the first cycle of both MoS_2/DWCNTs and MoS_2/Super P electrodes. In the discharge curves, the sloping plateau at ∼1.8 V corresponds to the onset of Li^+-ion insertion in MoS_2 (according to $MoS_2 + xLi^+ + xe^- \rightarrow Li_xMoS_2$). At ∼1.2 V versus Li^+/Li, Li^+-ions begin to react with S atoms to form a LiS_2 matrix in which Mo metallic clusters are embedded (according to $2Li^+ + S + 2e^- \rightarrow Li_2S$).[33] Below 0.5 V versus Li^+/Li is a deep conversion zone along with the formation of solid electrolyte interface (SEI). The MoS_2-DWCNT electrodes showed a specific capacity of ∼1400 mAh/g while the MoS_2-Super P delivered ∼900 mAh/g at 100 mA/g. With equal wt % of carbon additives used, the capacity obtained using DWCNTs corresponds to the theoretical value obtained by DFT simulation (see Figure 2a and further), and this is often attributed to the ability of CNTs to electrically connect the active particles as they convert into various discharge products that tend to decrease electron/ion conductivities. In addition, it was proposed on the basis of a quantum chemical calculation[34] that in MoS_2-CNT composites there is an energetic preference for effective charge-transfer from CNT to MoS_2.

In order to illustrate the MoS_2-Li-ion battery discharge process (lithiation), the lowest energy structures at each stoichiometry were reoptimized using harder pseudopotentials generated by CASTEP as detailed in Supporting Information section S2. From these structures we obtained the convex hull and average voltages, depicting the formation energies of more stable intermediate phases as reported in Figure 2b. We find MoS_2, $LiMoS_2$, Li_3MoS_2, Li_5MoS_2, Li_7MoS_2, and Li on the hull with $Li_5(MoS_2)_2$ and Li_4MoS_2 near to the hull, hence well within the error of DFT and expected to be accessible by thermal excitation at room temperature. The convex hull of Li_xMoS_2 can be described by three distinct regions, $x \leq 1$, $1 < x < 2.5$, and $x > 2.5$, characterizing MoS_2 battery discharge cycles. In the first region the lowest energy structures are all MoS_2-like with various concentrations of Li intercalated between the layers (Li-ion insertion zone). In the second region, clusters of MoS_2 with sulfur on the outside, directed toward the lithium, dominate (conversion zone). Finally, in the last region, sulfur is released from Mo. The sulfur bonds with the lithium, forming structures similar to Li_2S, and with the remaining Li and Mo, forming Li−Mo alloys (deep conversion zone). Thus, the MoS_2 electrodes undergo a series of conversion reactions with Li-ions as the battery is fully discharged at the end of first discharge cycle.

In Figure 2a,b, we find only one Li_3MoS_2 phase with low energy. It has $P2_1/c$ symmetry, and is clearly segregated into Li_2S-like and MoS-like regions. All low energy structures of Li_4MoS_2, Li_5MoS_2, and Li_6MoS_2 comprise regions of simple Mo chains and Li_2S-like regions. Evidently, DFT shows that at the start of lithiation (Li_xMoS_2 $x \leq 1$) this region comprises MoS_2 sheets with lithium intercalated between them. The $LiMo_3S_6$ stoichiometry's lowest energy structure has a $P6_3/mcm$ symmetry, and 0.024 eV/f.u. above it lies a $P6_322$ phase. Both

DOI: 10.1021/acs.chemmater.6b02607
Chem. Mater. 2016, 28, 7304−7310

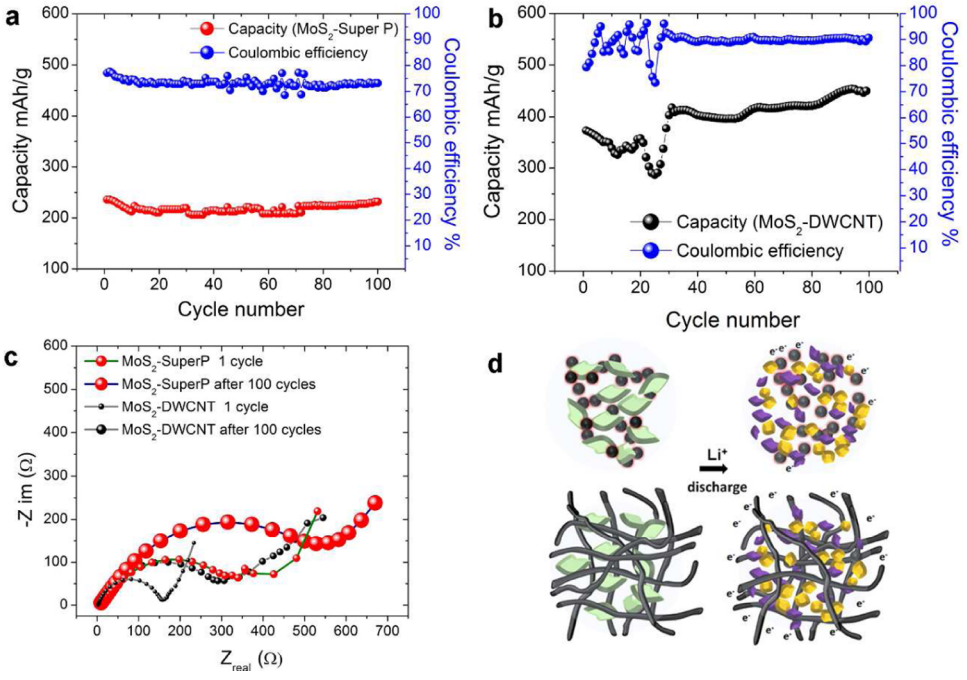

Figure 3. Cycling data: (a) MoS_2-Super P carbon, (b) MoS_2-DWCNTs, (c) electrochemical impedance analysis (EIS) of both types of electrodes, (d) schematics of a Super P carbon and CNT based electrode internal structures.

contain layers of MoS_2 sheets only differing in the lithium sites between adjacent layers. All of the lowest energy structures to at least 0.068 eV/f.u. above the ground state of $LiMo_2S_4$ were lithium intercalated MoS_2. All of which contain flat MoS_2 sheets except a *Cmcm* phase 0.014 eV/f.u. above the ground state which has buckled sheets (Figure 2a). The only $Li_2Mo_3S_6$ phase we found within the cutoff was a layered $P6_3/mcm$ phase. Also, in this region the lowest energy $LiMoS_2$ found by *ab initio* random structure searching was the known $P\bar{1}$ [15] layered phase. However, the electrodes do not suffer from severe structural distortions due to the lithiation of MoS_2 layers, similar to Li-ion insertion in commercial carbon anodes[35,36] but offer only one-third of its total capacity (~350 mAh/g).

After the Li^+-ions insertion, the second lithiation stage (Li_xMoS_2 $1 < x \leq 2.5$) is a region where MoS_2 mainly comprises clusters and chains. The lowest energy $Li_3Mo_2S_4$ and $Li_5Mo_2S_4$ structures belong to the I_4/mmm and $R\bar{3}$ space groups, respectively. They both comprise MoS_2 clusters, containing 6Mo and 12S atoms toward the outside (see Figure 2a). These are reminiscent of well-known Mo-halogen/chalcogen clusters, although these normally comprise 6 Mo and 14 halogen/chalcogen atoms. The former has eight 3-fold and four 1-fold coordinated sulfur atoms, whereas the latter has six 3-fold and six 1-fold coordinations, indicating sulfur's preference to bond with lithium, as lithium concentrations increase. The lowest energy Li_2MoS_2 phase contains MoS_2 chains and has $P\bar{1}$ symmetry. 0.018 eV/f.u. above the ground state is a C_2 phase containing similar clusters to the I_4/mmm phase mentioned above, but with clusters sharing some sulfur and containing one fewer Mo. As a result, the MoS_2 particles undergo a drastic structural and morphological change, which causes the active particles to lose their interconnectivities and detach from carbon additive as the active particles swell and disintegrate. Then, as the lithiation continues toward completion, DFT indicates a final region Li_xMoS_2 $2.5 < x -$ Li_2S where some sulfur atoms are bonded only to lithium. Therefore, in the battery this area appears to be highly amorphous, segregating into Li_2S-rich and Mo-rich regions, leading to severe structural discontinuities within electrodes. If carbon additives present in electrodes are not able to retain interparticle connectivity, the batteries show a rapid capacity fade and eventually fail. We find only one Li_3MoS_2 phase with low energy. It has $P2_1/c$ symmetry, and is clearly segregated into Li_2S-like and MoS-like regions (see Figure 2). All low energy structures of Li_4MoS_2, Li_5MoS_2, and Li_6MoS_2 comprise regions of simple Mo chains and Li_2S-like regions. Therefore, our DFT results reveal that, at the end of the first discharge, the MoS_2 electrodes lose their structural integrity and also accumulate sulfide-rich phases that tend to be electrochemically inactive and electric insulators[37] (sulfur $\sim 5 \times 10^{-30}$ S cm^{-1} compared to $1-4 \times 10^2$ S cm^{-1} of graphite).

In accordance with these DFT results, Figure 3a,b shows the cycling behavior of both the CNT and Super P electrodes. These electrodes were cycled at a high current density of ~2A/g which is sufficiently high to cause rapid structural changes of the electrodes and therefore to test the ability of carbon additives to cope with MoS_2 electrode reactions in the conversion zones (as in Figure 2ii,iii). DWCNT electrodes, with the equal loading of carbon additive as Super P carbon references, offer higher capacity and columbic efficiency (CE). The high capacity and CE of CNT electrodes indicates better kinetics and reversibility of the electrode reactions (Figure 3 a,b). Super P in the same loading by wt % apparently fails to stabilize the MoS_2 particles which disintegrate during conversion reactions, and tend to expose new surfaces which result in electrically inaccessible domains, which corroborates the measured low capacity and CE. In general, 10 wt % carbon additive is sufficient to achieve a good electrical percolation in electrodes at the start of battery cycling. However, for Super P carbon, this does not seem to compensate for the loss of electrical conduction due to the conversion reactions as described by our DFT analysis. For example, carbon content

DOI: 10.1021/acs.chemmater.6b02607
Chem. Mater. 2016, 28, 7304−7310

~>30% has widely been used in MoS_2 composite electrodes[38,39,28] for achieving high reversible capacity and cyclability, whereas MoS_2 electrodes containing ≤10 wt % carbon exhibited poor electrochemical activities and quick capacity fade.[40−42] Nevertheless, the use of carbon additives above 10% decreases volumetrically the loading of active particles, which decreases energy density of electrodes.

The MoS_2−CNT electrodes show a stable cycling performance (Figure 3b) despite undergoing an initial fluctuation regime where the electrodes experience dramatic structural changes and produce Li-polysulfides. For example, the amount of strain that is induced by the conversion reactions has been shown to cause cracks in MoS_2 electrodes, but CNTs prevent the complete electrical disruption by bridging cracks.[43] We note that the CE % fluctuation in cycling was found to be minimal at a low rate (Supporting Information). The fact that CNT electrodes (Figure 3b) are stabilized after initial fluctuations in galvanostatic cycling indicates that (i) the MoS_2 electrodes undergo a drastic structural rearrangement from the early cycles as confirmed by our DFT, and (ii) the converted electrode particles are then effectively stabilized by the CNT network. The sulfur-rich intermediates, apart from leading to severe disruption of the electrical network within electrodes, can also dissolve in battery electrodes or diffuse between electrodes,[44] and therefore, their stabilization is critical to the battery life which can be improved by using CNTs as conductive additives.

Finally, we performed electrochemical impedance analysis (EIS) to obtain information on the electrode impedance.[45] The representative EIS Nyquist plots in Figure 3c show that the electrode resistance is substantially lower (~145 Ω) for MoS_2-DWCNT than MoS_2-Super P carbon (~350 Ω). We therefore conclude that CNTs offer a highly conductive scaffold (Figure 3d) that enhances the electrical conduction throughout battery cycling and increases the utility of Li polysulfide phases, resulting in high capacity and Coulombic efficiency.

■ CONCLUSION

This paper presents new insights into the chemistry of a conversion-type MoS_2 nanosheet for Li-ion batteries. Using DFT simulations, we show that the Li-MoS_2 phase diagram is very rich, especially for higher lithium concentration regions. *Ab initio* random structure searching predicts a series of Li-polysulfide intermediates for a wide range of stoichiometries. These sulfur-rich intermediates progressively insulate the MoS_2 electrodes, and to cope with this, the choice of the conductive additive is critical. By benchmarking CNTs against Super P carbon, the ability of CNTs to stabilize conversion reactions is evidenced. We measured a 45% reduction in electrode resistance, a nearly 2-fold increase in capacity, and Coulombic efficiencies of over 90%. Our results on MoS_2 phase transformation and the role of CNT additives in these batteries will facilitate the adoption of metal sulfide electrodes in high energy density batteries.

■ EXPERIMENTAL SECTION

Materials. Commercial DWCNTs (NC2000) were purchased from Nanocyl s.a. and used without any pretreatment. MoS_2 crystals (micron sized) were obtained from Acros-Organics. Electrochemical grade propylene carbonate, ethylene carbonate, diethyl carbonate, *N*-methyl-2-pyrrolidone, polyvinylidene fluoride (PVDF), and Li metal foils were purchased from Sigma-Aldrich. Carbon powder (carbon Super P) was purchased from Alfa Aesar. Polypropylene layers were purchased from Cell Guard.

Exfoliation of MoS_2. MoS_2 crystals were exfoliated followed by a method described elsewhere.[46] Briefly, MoS_2 crystals were mixed with *N*-methyl-2-pyrrolidone (NMP) and sonicated leading to a dispersion of MoS_2 nanosheets. The resultant dispersion was centrifuged and redispersed in fresh NMP. The suspension was kept still for several hours to allow for the precipitation of partially exfoliated MoS_2 fragments, and this process was repeated a number of times until a clear suspension containing MoS_2 nanosheets with an average thickness of 7 nm was achieved.

Li-Ion Battery Fabrication. Commercial DWCNT powder was added to MoS_2 nanosheets, and then mixed with PVDF in a weight ratio of 10:85:5 in NMP. The composite formed a thick slurry which then was coated onto a copper current collector and dried at 120 °C for 12 h. The 2032-type cells were assembled using a MoS_2-CNT-PVDF slurry coated electrode, and pure Li metal was used both as reference and counter electrode. Polypropylene layers were used to separate the electrodes, and 1 M LiF_6P in diethyl carbonate and dimethyl carbonate in volume ratio 1:1 was used as electrolyte.

Instrumentation. Scanning electron microscopy (SEM) images were acquired using a Leo Variable pressure SEM. High resolution transmission electron microscopy (HRTEM) measurements were carried out using an FEI Tecnai F20 operating under 200 kV field emission gun (FEG). UV−vis−NIR optical absorption spectroscopy was carried out using a PerkinElmer lambda 750 UV−vis−NIR instrument. All electrochemical measurements were carried out by using a VMP3 multichannel potentiostat/battery cycler equipped with a 5A current booster from Biologics. Raman measurements were carried out using a EZRAMAN-N instrument on films of samples on Si substrates. X-ray diffraction (XRD) measurements were carried out by using a Bruker D8 θ/θ (fixed sample) instrument with a position sensitive detector (LynxEye) and standard detector (SC).

DFT Simulation. To predict the likely structures of Li_xMoS_2 that form during lithiation, we used the *ab initio* random structure searching (AIRSS) method.[47,48] AIRSS has successfully predicted the structures of phases of Li-ion batteries (LIBs) containing sulfur,[49] phosphorus,[50] silicon, and germanium.[51] Not limited to ground-state crystal structures, AIRSS has been used to understand point defects[52] and continuous phase transitions in LIBs.[53] AIRSS searches were carried out on stoichiometries of $Li_xMo_yS_{2y}$ at ratios of less than of 8:1 of Li:MoS_2 which corresponds to a theoretical capacity of up to 1688 mAh/g. To limit the number of atoms in the simulation cells, stoichiometries were constrained to $x + 3y \leq 11$. Initial searches were carried out using the CASTEP 8.03 DFT code with the PBE[54] exchange-correlation functional and Vanderbilt "ultra-soft" pseudopotentials. The Brillouin zone (BZ) was integrated using a Monkhost−Pack grid spacing of $2\pi \times 0.05$ Å^{-1} or better. The basis set contained plane waves up to 300 eV. The stable structures at zero temperature were obtained by plotting the fractional atomic composition against the formation energy per atom (see SI section S2) and drawing a convex hull around the points from 0, 0 to 0, 1. The stable structures lie on these tie lines. To obtain the formation energies and average voltages, the lowest energy structures at each stoichiometry were reoptimized using harder pseudopotentials generated by CASTEP as detailed in Supporting Information section S1.

■ ASSOCIATED CONTENT

Supporting Information

The Supporting Information is available free of charge on the ACS Publications website at DOI: 10.1021/acs.chemmater.6b02607.

Additional details on *ab initio* density-functional theory (DFT) analysis, SEM image of the cross section of a MoS_2-DWCNTs electrode, and additional electrochemical data on the Coulombic efficiency of MoS_2-DWCNTs at a low rate. Additional data related to this publication is available at the University of Cambridge data repository http://dx.doi.org/10.17863/CAM.4480 (PDF)

DOI: 10.1021/acs.chemmater.6b02607
Chem. Mater. 2016, 28, 7304−7310

AUTHOR INFORMATION

Corresponding Authors

*E-mail: gc495@cam.ac.uk.
*E-mail: ajm255@cam.ac.uk.
*E-mail: mfld2@cam.ac.uk.

Author Contributions

§C.G. and A.J.M. equally contributed to this work.

Notes

The authors declare no competing financial interest.

ACKNOWLEDGMENTS

C.G and M.D.V acknowledge the support from ERC starting grant 337739-HIENA. A.J.M. acknowledges the support from the Winton Programme for the Physics of Sustainability. Computational resources were provided by the Cambridge High Performance Computing service. M.H.M acknowledges the support from EPSRC Cambridge NanoDTC, EP/G037221/1. The authors thank R. J. Needs, D. R. Bowler, M. D. Mayo, Dr. T Hasan. and G. Hu for insightful discussions.

REFERENCES

(1) Savjani, N.; Lewis, E. a.; Pattrick, R. a. D.; Haigh, S. J.; O'Brien, P. MoS_2 Nanosheet Production by the Direct Exfoliation of Molybdenite Minerals from Several Type-Localities. *RSC Adv.* **2014**, *4*, 35609.

(2) Tsai, M.-L.; Su, S.-H.; Chang, J.-K.; Tsai, D.-S.; Chen, C.-H.; Wu, C.-I.; Li, L.-J.; Chen, L.-J.; He, J.-H. Monolayer MoS_2 Heterojunction Solar Cells. *ACS Nano* **2014**, *8*, 8317−8322.

(3) Lopez-Sanchez, O.; Lembke, D.; Kayci, M.; Radenovic, A.; Kis, A. Ultrasensitive Photodetectors Based on Monolayer MoS_2. *Nat. Nanotechnol.* **2013**, *8*, 497−501.

(4) Ye, L.; Wu, C.; Guo, W.; Xie, Y. MoS_2 Hierarchical Hollow Cubic Cages Assembled by Bilayers: One-Step Synthesis and Their Electrochemical Hydrogen Storage Properties. *Chem. Commun.* **2006**, *45*, 4738−4740.

(5) Lukowski, M. A.; Daniel, A. S.; Meng, F.; Forticaux, A.; Li, L.; Jin, S. Enhanced Hydrogen Evolution Catalysis from Chemically Exfoliated Metallic MoS_2 Nanosheets. *J. Am. Chem. Soc.* **2013**, *135*, 10274−10277.

(6) Stephenson, T.; Li, Z.; Olsen, B.; Mitlin, D. Lithium Ion Battery Applications of Molybdenum Disulfide (MoS_2) Nanocomposites. *Energy Environ. Sci.* **2014**, *7*, 209−231.

(7) Cao, L.; Yang, S.; Gao, W.; Liu, Z.; Gong, Y.; Ma, L.; Shi, G.; Lei, S.; Zhang, Y.; Zhang, S.; Vajtai, R.; Ajayan, P. M. Direct Laser-Patterned Micro-Supercapacitors from Paintable MoS_2 Films. *Small* **2013**, *9*, 2905−2910.

(8) Radisavljevic, B.; Radenovic, A.; Brivio, J.; Giacometti, V.; Kis, A. Single-Layer MoS_2 Transistors. *Nat. Nanotechnol.* **2011**, *6*, 147−150.

(9) Chhowalla, M.; Amaratunga, G. Thin Films of Fullerene-like MoS_2 Nanoparticles with Ultra-Low Friction and Wear. *Nature* **2000**, *407*, 164−167.

(10) Xiao, J.; Choi, D.; Cosimbescu, L.; Koech, P.; Liu, J.; Lemmon, J. P. Exfoliated MoS_2 Nanocomposite as an Anode Material for Lithium Ion Batteries. *Chem. Mater.* **2010**, *22*, 4522−4524.

(11) Zhang, L.; Wu, H. B.; Yan, Y.; Wang, X.; Lou, X. W. D. Hierarchical MoS_2 Microboxes Constructed by Nanosheets with Enhanced Electrochemical Properties for Lithium Storage and Water Splitting. *Energy Environ. Sci.* **2014**, *7*, 3302−3306.

(12) Goriparti, S.; Miele, E.; De Angelis, F.; Di Fabrizio, E.; Proietti Zaccaria, R.; Capiglia, C. Review on Recent Progress of Nanostructured Anode Materials for Li-Ion Batteries. *J. Power Sources* **2014**, *257*, 421−443.

(13) Liu, N.; Kim, P.; Kim, J. H.; Ye, J. H.; Kim, S.; Lee, C. J. Large-Area Atomically Thin MoS_2 Nanosheets Prepared Using Electrochemical Exfoliation. *ACS Nano* **2014**, *8*, 6902−6910.

(14) Lu, Y.; Yao, X.; Yin, J.; Peng, G.; Cui, P.; Xu, X. MoS_2 Nanoflowers Consisting of Nanosheets with a Controllable Interlayer Distance as High-Performance Lithium Ion Battery Anodes. *RSC Adv.* **2015**, *5*, 7938−7943.

(15) Wang, L.; Xu, Z.; Wang, W.; Bai, X. Atomic Mechanism of Dynamic Electrochemical Lithiation Processes of MoS_2 Nanosheets. *J. Am. Chem. Soc.* **2014**, *136*, 6693−6697.

(16) Diao, Y.; Xie, K.; Xiong, S.; Hong, X. Analysis of Polysulfide Dissolved in Electrolyte in Discharge-Charge Process of Li-S Battery. *J. Electrochem. Soc.* **2012**, *159*, A421.

(17) Suo, L.; Hu, Y.-S.; Li, H.; Armand, M.; Chen, L. A New Class of Solvent-in-Salt Electrolyte for High-Energy Rechargeable Metallic Lithium Batteries. *Nat. Commun.* **2013**, *4*, 1481.

(18) Li, X.; Kang, F.; Bai, X.; Shen, W. A Novel Network Composite Cathode of $LiFePO_4$/multiwalled Carbon Nanotubes with High Rate Capability for Lithium Ion Batteries. *Electrochem. Commun.* **2007**, *9*, 663−666.

(19) Evanoff, K.; Khan, J.; Balandin, A. A.; Magasinski, A.; Ready, W. J.; Fuller, T. F.; Yushin, G. Towards Ultrathick Battery Electrodes: Aligned Carbon Nanotube-Enabled Architecture. *Adv. Mater.* **2012**, *24*, 533−537.

(20) Bindumadhavan, K.; Srivastava, S. K.; Mahanty, S. MoS_2-MWCNT Hybrids as a Superior Anode in Lithium-Ion Batteries. *Chem. Commun.* **2013**, *49*, 1823−1825.

(21) Li, J.; Hou, Y.; Gao, X.; Guan, D.; Xie, Y.; Chen, J.; Yuan, C. A Three-Dimensionally Interconnected Carbon Nanotube/layered MoS_2 Nanohybrid Network for Lithium Ion Battery Anode with Superior Rate Capacity and Long-Cycle-Life. *Nano Energy* **2015**, *16*, 10−18.

(22) Chen, Y. M.; Yu, X. Y.; Li, Z.; Paik, U.; Wen, X.; Lou, X. W. D. Hierarchical MoS_2 Tubular Structures Internally Wired by Carbon Nanotubes as a Highly Stable Anode Material for Lithium-Ion Batteries. *Sci.Adv.* **2016**, *2*, e1600021.

(23) Yu, X.-Y.; Hu, H.; Wang, Y.; Chen, H.; Lou, X. W. D. Ultrathin MoS2 Nanosheets Supported on N-Doped Carbon Nanoboxes with Enhanced Lithium Storage and Electrocatalytic Properties. *Angew. Chem., Int. Ed.* **2015**, *54*, 7395−7398.

(24) Yang, L.; Wang, S.; Mao, J.; Deng, J.; Gao, Q.; Tang, Y.; Schmidt, O. G. Hierarchical MoS_2/polyaniline Nanowires with Excellent Electrochemical Performance for Lithium-Ion Batteries. *Adv. Mater.* **2013**, *25*, 1180−1184.

(25) Sen, U. K.; Mitra, S. High-Rate and High-Energy-Density Lithium-Ion Battery Anode Containing 2D MoS_2 Nanowall and Cellulose Binder. *ACS Appl. Mater. Interfaces* **2013**, *5*, 1240−1247.

(26) Chang, K.; Chen, W. L -Cysteine-Assisted Synthesis of Layered MoS_2/graphene Composites with Excellent Electrochemical Performances for Lithium Ion Batteries. *ACS Nano* **2011**, *5*, 4720−4728.

(27) Zhang, C.; Wu, H. B.; Guo, Z.; Lou, X. W. D. Facile Synthesis of Carbon-Coated MoS_2 Nanorods with Enhanced Lithium Storage Properties. *Electrochem. Commun.* **2012**, *20*, 7−10.

(28) Xu, X.; Fan, Z.; Yu, X.; Ding, S.; Yu, D.; Lou, X. W. D. A Nanosheets-on-Channel Architecture Constructed from MoS_2 and CMK-3 for High-Capacity and Long-Cycle-Life Lithium Storage. *Adv. Energy Mater.* **2014**, *4*, 1400902.

(29) Hwang, H.; Kim, H.; Cho, J. MoS2 Nanoplates Consisting of Disordered Graphene-like Layers for High Rate Lithium Battery Anode Materials. *Nano Lett.* **2011**, *11*, 4826−4830.

(30) Wang, L.; Xu, Z.; Wang, W.; Bai, X. Atomic Mechanism of Dynamic Electrochemical Lithiation Processes of MoS_2 Nanosheets. *J. Am. Chem. Soc.* **2014**, *136*, 6693−6697.

(31) Xiao, J.; Wang, X.; Yang, X. Q.; Xun, S.; Liu, G.; Koech, P. K.; Liu, J.; Lemmon, J. P. Electrochemically Induced High Capacity Displacement Reaction of PEO/MoS_2/graphene Nanocomposites with Lithium. *Adv. Funct. Mater.* **2011**, *21*, 2840−2846.

(32) Sen, U. K.; Johari, P.; Basu, S.; Nayak, C.; Mitra, S. An Experimental and Computational Study to Understand the Lithium Storage Mechanism in Molybdenum Disulfide. *Nanoscale* **2014**, *6*, 10243−10254.

(33) Sharma, N.; Du, G.; Studer, A. J.; Guo, Z.; Peterson, V. K. In-Situ Neutron Diffraction Study of the MoS_2 Anode Using a Custom-Built Li-Ion Battery. *Solid State Ionics* **2011**, *199*−*200*, 37−43.

DOI: 10.1021/acs.chemmater.6b02607
Chem. Mater. 2016, 28, 7304−7310

(34) Koroteev, V. O.; Bulusheva, L. G.; Asanov, I. P.; Shlyakhova, E. V.; Vyalikh, D. V.; Okotrub, A. V. Charge Transfer in the MoS_2/carbon Nanotube Composite. *J. Phys. Chem. C* **2011**, *115*, 21199−21204.
(35) Tran, T. D.; Feikert, J. H.; Song, X.; Kinoshita, K. Commercial Carbonaceous Materials as Lithium Intercalation Anodes. *J. Electrochem. Soc.* **1995**, *142*, 3297−3302.
(36) Dahn, J. R.; Zheng, T.; Liu, Y.; Xue, J. S. Mechanisms for Lithium Insertion in Carbonaceous Materials. *Science* **1995**, *270*, 590−593.
(37) Fan, F. Y.; Carter, W. C.; Chiang, Y.-M. Mechanism and Kinetics of Li_2S Precipitation in Lithium−Sulfur Batteries. *Adv. Mater.* **2015**, *27*, 5203−5209.
(38) Zhu, C.; Mu, X.; Vanaken, P. A.; Yu, Y.; Maier, J. Single-Layered Ultrasmall Nanoplates of MoS_2 Embedded in Carbon Nanofibers with Excellent Electrochemical Performance for Lithium and Sodium Storage. *Angew. Chem., Int. Ed.* **2014**, *53*, 2152−2156.
(39) Wang, M.; Li, G.; Xu, H.; Qian, Y.; Yang, J. Enhanced Lithium Storage Performances of Hierarchical Hollow MoS_2 Nanoparticles Assembled from Nanosheets. *ACS Appl. Mater. Interfaces* **2013**, *5*, 1003−1008.
(40) Miao, Y. E.; Huang, Y. P.; Zhang, L. S.; Fan, W.; Lai, F. L.; Liu, T. X. Electrospun Porous Carbon nanofiber@MoS_2 Core/sheath Fiber Membranes as Highly Flexible and Binder-Free Anodes for Lithium-Ion Batteries. *Nanoscale* **2015**, *7*, 11093−11101.
(41) Zhou, J.; Qin, J.; Zhang, X.; Shi, C.; Liu, E.; Li, J.; Zhao, N.; He, C. 2D Space-Confined Synthesis of Few-Layer MoS_2 Anchored on Carbon Nanosheet for Lithium-Ion Battery Anode. *ACS Nano* **2015**, *9*, 3837−3848.
(42) Pham, V. H.; Kim, K.-H.; Jung, D.-W.; Singh, K.; Oh, E.-S.; Chung, J. S. Liquid Phase Co-Exfoliated MoS_2−graphene Composites as Anode Materials for Lithium Ion Batteries. *J. Power Sources* **2013**, *244*, 280−286.
(43) Liu, Y.; He, X.; Hanlon, D.; Harvey, A.; Khan, U.; Li, Y.; Coleman, J. N. Electrical, Mechanical and Capacity Percolation Leads to High Performance MoS_2 /Nanotube Composite Lithium Ion Battery Electrodes. *ACS Nano* **2016**, *10*, 5980−5990.
(44) Ji, X.; Evers, S.; Black, R.; Nazar, L. F. Stabilizing Lithium-Sulphur Cathodes Using Polysulphide Reservoirs. *Nat. Commun.* **2011**, *2*, 325.
(45) Dilena, E.; Dorfs, D.; George, C.; Miszta, K.; Povia, M.; Genovese, A.; Casu, A.; Prato, M.; Manna, L. Colloidal $Cu_{2-x}(S_ySe_{1-y})$ Alloy Nanocrystals with Controllable Crystal Phase: Synthesis, Plasmonic Properties, Cation Exchange and Electrochemical Lithiation. *J. Mater. Chem.* **2012**, *22*, 13023.
(46) Woodward, R. I.; Kelleher, E. J. R.; Howe, R. C. T.; Hu, G.; Torrisi, F.; Hasan, T.; Popov, S. V.; Taylor, J. R. Tunable Q-Switched Fiber Laser Based on Saturable Edge-State Absorption in Few-Layer Molybdenum Disulfide (MoS_2). *Opt. Express* **2014**, *22*, 31113.
(47) Pickard, C. J.; Needs, R. J. High-Pressure Phases of Silane. *Phys. Rev. Lett.* **2006**, *97*, 045504.
(48) Pickard, C. J.; Needs, R. J. Ab Initio Random Structure Searching. *J. Phys.: Condens. Matter* **2011**, *23*, 053201.
(49) See, K. A.; Leskes, M.; Griffin, J. M.; Britto, S.; Matthews, P. D.; Emly, A.; Van der Ven, A.; Wright, D. S.; Morris, A. J.; Grey, C. P.; Seshadri, R. Ab Initio Structure Search and in Situ ^{7}Li NMR Studies of Discharge Products in the Li − S Battery System. *J. Am. Chem. Soc.* **2014**, *136*, 16368−16377.
(50) Mayo, M.; Griffith, K. J.; Pickard, C. J.; Morris, A. J. Ab Initio Study of Phosphorus Anodes for Lithium- and Sodium-Ion Batteries. *Chem. Mater.* **2016**, *28*, 2011−2021.
(51) Morris, A. J.; Grey, C. P.; Pickard, C. J. Thermodynamically Stable Lithium Silicides and Germanides from Density Functional Theory Calculations. *Phys. Rev. B: Condens. Matter Mater. Phys.* **2014**, *90*, 054111.
(52) Morris, A. J.; Needs, R. J.; Salager, E.; Grey, C. P.; Pickard, C. J. Lithiation of Silicon via Lithium Zintl-Defect Complexes from First Principles. *Phys. Rev. B: Condens. Matter Mater. Phys.* **2013**, *87*, 174108.
(53) Jung, H.; Allan, P. K.; Hu, Y.-Y.; Borkiewicz, O. J.; Wang, X.-L.; Han, W.-Q.; Du, L.-S.; Pickard, C. J.; Chupas, P. J.; Chapman, K. W.; Morris, A. J.; Grey, C. P. Elucidation of the Local and Long-Range Structural Changes That Occur in Germanium Anodes in Lithium-Ion Batteries. *Chem. Mater.* **2015**, *27*, 1031−1041.
(54) Perdew, J. P.; Burke, K.; Ernzerhof, M. of Physics, D.; Quantum Theory Group Tulane University, N. O. L. 70118 J. Generalized Gradient Approximation Made Simple. *Phys. Rev. Lett.* **1996**, *77*, 3865−3868.

DOI: 10.1021/acs.chemmater.6b02607
Chem. Mater. 2016, 28, 7304−7310